MODELLING FOR AILERON INDUCED UNSTEADY AERODYNAMIC EFFECTS FOR PARAMETER ESTIMATION

Jatinder Singh and S.C. Raisinghani
Department of Aerospace Engineering
I.I.T. Kanpur, India

Abstract

Aileron inputs give rise to a trailing vortex pattern which is a function of time. To account for the unsteady aerodynamic effects due to such a vortex pattern, a model based on a simple vortex system is proposed. Expressions for the induced sidewash and downwash angles are derived and recast into a form which can be conveniently used in the equations of motion for parameter estimation. Maximum–likelihood method in frequency–domain is utilized to analyse the frequency response curves of an example airplane. Parameter estimation is carried out with and without the inclusion of unsteady aerodynamic modelling in the estimation model. For the latter case, an explanation is provided for the significant differences observed in the aileron control derivatives when unsteady aerodynamic modelling was omitted fully or partially.

Nomenclature

a_v, a_t	lift curve slope of the vertical and horizontal tail
a_y	linear acceleration along y-axis, g units
b	wing span, m
c	chord, m
$C_{L_t}, \Delta C_{L_t}$	lift and indicial lift coefficient of horizontal tail
$C_{L_{\delta_a}}$	aileron control derivative, $\partial C_L / \partial \delta_a$
C_y	sideforce coefficient of vertical tail
Ei( )	exponential integral of variable $\int_{-\infty}^{x} \frac{e^t}{t}\, dt$ (ref. 9)
g	accelration due to gravity, 9.8 m/sec^2
I_x, I_z	moment of inertia about X and Z axis
j	$\sqrt{-1}$
l_v, l	vertical and horizontal tail length, m
m	mass of the airplane, Kg
p, r	roll and yaw rate, rad/sec or deg/sec
S_w, S_v, S_t	wing, vertical tail and horizontal tail area, m^2
t, τ	time, sec
u	free stream velocity, m/sec
y, z	constants in indicial sideforce Eq. (4)
$\bar{y}$	distance from c.g. to a.c. of the left and right panels of the horizontal tail, m
z_v	vertical height of a.c. of vertical tail from c.g. of the aircraft
α	angle of attack at the wing, deg or rad
α_δ	aileron deflection parameter, $\partial \alpha / \partial \delta_a$ (ref. 8)
β	angle of sideslip, rad
δ_a, δ_r	aileron and rudder deflection, deg or rad
Λ	wing sweep, deg
ρ	density of air, Kg/m^3
$\Delta\epsilon$	indicial downwash angle, deg or rad
$\Delta\sigma$	indicial sidewash angle, deg or rad
ϕ	bank angle, deg or rad
ω	angular frequency, rad/sec
∞	infinity

Superscripts

$\bar{\ }$	mean value
$\dot{\ }$	derivative with respect to time
$\sim$	Fourier transform
T	transpose of a matrix
′	total derivatives
″	equivalent derivatives

Subscripts

r	root
ss	steady state value
t	horizontal tail
v	vertical tail
w	wing

Abbreviations

a.c.	aerodynamic center
c.g.	center of gravity

Introduction

Estimation algorithms based only on quasisteady flow theory have been observed to cause additional uncertainity in parameter estimates[1]. This has resulted in efforts being expended at modelling of unsteady aerodynamic effects into aircraft equations of motion for parameter estimation. The simplest way to account for these unsteady effects in aircraft dynamics is through an aerodynamic force model based on physical principle of Prandtl's lifting line theory and trailing vortex concept[2]. Of late, this concept has been extensively used to modify longitudinal[3,4] and lateral[5,6] equations of motion for parameter estimation.

The purpose of the present study is to develop simple concepts which would permit modelling of unsteady aerodynamic effects arising from the vortex pattern from aileron input into parameter extraction algorithm. Such modelling is expected to lead to increased confidence and high fidelity in parameter estimates. Frequency response curves for unit aileron impulse input are computer generated for an example airplane. Maximum likelihood method in frequency–domain is utilized for parameter estimation from frequency response to show the effect of unsteady aerodynamics on estimated parameters. The aileron control derivatives are found to be the most affected, showing marked variance from their true values.

Simplified Asymmetric Vortex Pattern

A simplified arrangement of vortex pattern for a full span positive aileron deflection is shown in Fig. 1. Unlike the vortex system used heretofore for estimation purposes[4,5], the proposed vortex system assumes a vortex pattern for each panel of the wing due to effective angle of attack change caused by deflection of aileron surface on that panel. The vortices have the direction as shown in Fig. 1 and the same circulation strength Γ as determined by the lift generated on each panel given by $C_{L_{\delta_a}} \delta_a / 2$.

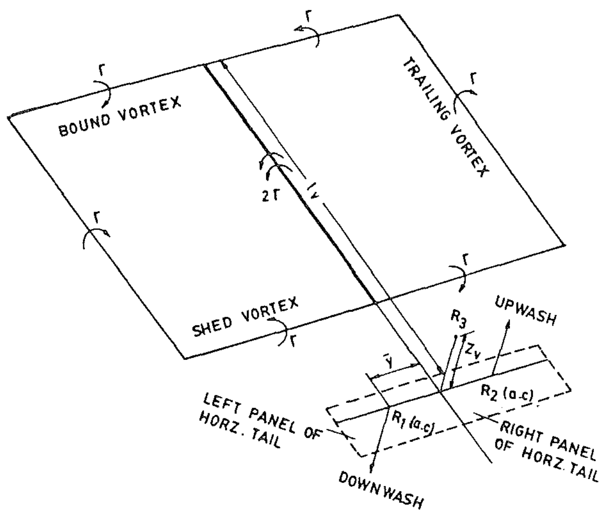

FIG. 1 ASYMMETRIC VORTEX PATTERN DUE TO POSITIVE AILERON INPUT

Induced velocities are calculated at the a.c. of the left panel (R_1) and right panel (R_2) of the horizontal tail, and also at the a.c. (R_3) of the vertical tail (Fig.1). The trailing vortices are assumed to move in the plane of the wing and at one-half the free stream velocity[3]. Biot-Savart law can now be used to calculate the induced velocities and thereby induced angles at the tail surfaces.

Using Biot-Savart law, the sidewash at the a.c. of the vertical tail due to the vortex system in Fig. 1 is given by

$$\sigma(t) = -\frac{2C_L(t)\bar{c}\,z_V}{8\pi}\left[f_1(t)+f_2(t)+f_3(t)+f_4(t)\right] \qquad (1)$$

where functions $f_1, \cdots, f_4$ are defined in Appendix A.

Even though the vortex model shown in Fig. 1 is a highly simplified representation of a complex physical system, Eq. (1) gives a useful relationship between sidewash and time for varying aileron input. For unit step increase in aileron input, the indicial sidewash angle is given by

$$\Delta\sigma(t) = -\frac{2\Delta C_L(t)\bar{c}\,z_V}{8\pi}\left[f_1(t)+f_2(t)+f_3(t)+f_4(t)\right] \quad (2)$$

where the indicial lift coefficient[2] for a unit step δ_a input is given by

$$\Delta C_L(t) = (C_{L_{\delta_a}})_{ss}\left[1 - y\,\exp\left(-\frac{2zut}{c_r}\right)\right] \qquad (3)$$

The constants y and z in the above expression are function of wing geomtry, and their values are obtained using the vortex pattern representing each panel of the wing. Under steady state conditions Eq. (2) becomes

$$(\Delta\sigma)_{SS} = -\frac{2(C_{L_{\delta_a}})_{SS}\,\bar{c}\,z_V}{8\pi}\left[f_1(\infty)+f_2(\infty)+f_3(\infty)+f_4(\infty)\right] \quad (4)$$

Combining equations (2) and (4), we obtain

$$\Delta\sigma(t) = \left(\frac{d\sigma}{d\delta_a}\right)_{SS}\left[1 - y\exp\left(-\frac{2zut}{c_r}\right)\right] \times \left[\frac{f_1(t)+f_2(t)+f_3(t)+f_4(t)}{f_1(\infty)+f_2(\infty)+f_3(\infty)+f_4(\infty)}\right] \qquad (5)$$

A similar expression for the induced indicial downwash is obtained using Biot-Savart law to the asymmetric vortex system in Fig.1 which induces a downwash on the left panel (looking from behind) and an equal amount of upwash on the right panel of the horizontal tail. The induced indicial downwash angle at the a.c. of the left panel is given by

$$\epsilon(t) = \frac{C_L(t)\bar{c}}{8\pi}\left[g_1(t)+g_2(t)+g_3(t)+g_4(t)+g_5(t)+g_6(t)+g_7(t)\right] \qquad (6)$$

where functions $g_1, \ldots, g_7$ are defined in Appendix B. The accuracy of the above expression is improved by ensuring its correctness at the known steady state conditions[3,4]. For a unit step increase in aileron input δ_a, the indicial downwash angle $\Delta\epsilon$ under steady state conditions is given by

$$(\Delta\epsilon)_{SS} = \left(\frac{d\epsilon}{d\alpha}\right)_{l,SS} = \frac{(C_{L_{\delta_a}})_{SS}\,\bar{c}}{8\pi}\left[g_1(\infty)+\ldots+g_7(\infty)\right] \qquad (7)$$

Combining equations (6) and (7), we obtain

$$\Delta\epsilon(t) = \left(\frac{d\epsilon}{d\alpha}\right)_{l,SS}\alpha_\delta\left[1 - y\exp\left(-\frac{2zut}{c_r}\right)\right]\left[\frac{g_1(t)+\ldots+g_7(t)}{g_1(\infty)+\ldots+g_7(\infty)}\right] \qquad (8)$$

Other than the unsteady effects in sidewash and downwash given by equations (5) and (8), lift build up at the horizontal and vertical tails also contribute to the unsteady aerodynamic effects. As suggested in refs.4 and 5, expressions similar to Eq.(3) for the indicial lift build up can be used to model such effects, e.g., the sideforce build up at the vertical tail can be modelled by the indicial sideforce function

$$\Delta C_y = -a_V\left[1 - y\exp\left(-\frac{2zut}{c_V}\right)\right] \qquad (9)$$

However, a brief study suggested that the effects of the unsteady aerodynamics on aircraft motion could be modelled reasonably accurately even if the load build up in lift and sideforce were omitted while the contribution due to lag in downwash and sidewash were retained (Fig. 4 discussed later). In keeping with this simplification, the load build up effects have therefore been omitted from further analysis (y=z=0 in Eqs. 5 and 8) .

The expressions for the induced indicial sidewash and downwash angles in Eqs. (5) and (8) are very long and cumbersome and as such not in a suitable form for use in aircraft equations of motion for parameter estimation. To that purpose, $\Delta\sigma$ and $\Delta\epsilon$ were calculated for a few specific cases and after some trials, the following expressions for the induced angles were observed to approximate equations (5) and (8) reasonably accurately

$$\Delta\sigma(t)=\left(\frac{d\sigma}{d\delta_a}\right)_{ss}\left[1-D\exp\left(-\frac{2Eut^2+2Fl_v t}{c_r}\right)\right] \quad (10)$$

$$\Delta\epsilon(t)=\left(\frac{d\epsilon}{d\alpha}\right)_{l,ss}\alpha_\delta \times\left[1-\frac{Lc_r}{(1-\bar{y}\tan\Lambda)-(ut/2)-c_r}-M\exp\left(-\frac{2Nut}{c_r}\right)\right] \quad (11)$$

Constants D, E and F in Eq.(10) and L, M and N in Eq.(11) are function of wing and tail geometry and location. These are obtained by curve fitting Eq. (10) to Eq. (5), and Eq. (11) to Eq. (8). Figure 2 and Fig. 3, respectively, show the exact and approximate time histories of the indicial sidewash and downwash angles for $\Lambda=0°$.

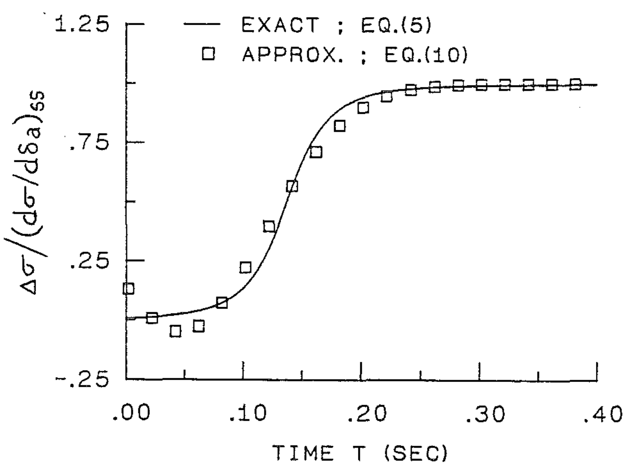

FIG. 2 EXACT AND APPROXIMATE TIME HISTORIES FOR INDICIAL SIDEWASH

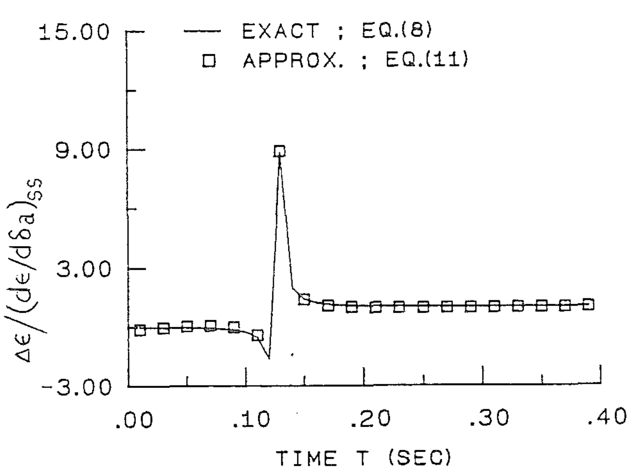

FIG. 3 EXACT AND APPROXIMATE TIME HISTORIES FOR INDICIAL DOWNWASH

In Fig. 2, except for the region very near to origin, the matching is reasonably good. Parameters $\left(\frac{d\epsilon}{d\alpha}\right)_{l,ss}$ and α_δ were calculated from refs. 7 and 8. Since accurate methods for computing $\left(\frac{d\sigma}{d\delta_a}\right)_{ss}$ were not readily available, its value was obtained from Eq.(4). In comparison to Eqs. (5) and (8), Eqs. (10) and (11) now give much simplified expressions for $\Delta\sigma$ and $\Delta\epsilon$ which are amenable to laplace transform and, therefore, can be conveniently used in equations of motion for parameter estimation.

The induced forces for arbitrary angle of attack at the tail surfaces are obtained using Duhamel's integral

$$C_y(t)=\int_0^t \Delta C_y(t-\tau)\,[\dot\beta(\tau)+\Delta\dot\sigma(\tau)]\,d\tau \quad (12)$$

$$C_{L_t}(t)=\int_0^t \Delta C_{L_t}(t-\tau)\,[\dot\alpha(\tau)\pm\Delta\dot\epsilon(\tau)]\,d\tau \quad (13)$$

where + and − signs are, respectively, for the upwash on the right panel and downwash on the left panel of the horizontal stabilator.

To avoid lengthy computations, it was found expedient to transform the above integro-differential equations into the frequency-domain for parameter estimation. This can be achieved by obtaining Laplace transform of Eqs. (10—13) and then substituting $s=j\omega$. The Laplace transform yields

$$\Delta\sigma(s)=\left(\frac{d\sigma}{d\delta_a}\right)_{ss}[1-D_1(s)] \quad (14)$$

$$\Delta\epsilon(s)=\left(\frac{d\epsilon}{d\alpha}\right)_{l,ss}[1-D_2(s)] \quad (15)$$

$$C_y(s)=-a_v\,[\beta(s)+\Delta\sigma(s)] \quad (16)$$

$$C_{L_t}(s)=a_t\,[\alpha(s)\pm\Delta\epsilon(s)] \quad (17)$$

Functions D_1 and D_2 are defined as follows :

$$D_1(s)=\frac{Ds}{2}\sqrt{\pi/f}\;\exp\left[(h+s)^2/4f\right]\operatorname{erfc}\left[(h+s)/2\sqrt{f}\right]$$

where $f=2Eu/c_r$; $h=2Fl_v/c_r$ and erfc is complementary error function[3]. Constants D, E and F are as defined in Eq.(10)

$$D_2(s)=\frac{Ms}{s+(2Nu/c_r)}+\frac{2sLc_r}{u}\exp(-m)\,Ei(m)$$

where Ei is the exponential integral[3] and

$$m=2s\left[1-\bar{y}\tan\Lambda-c_r\right]/u$$

Constants L, M and N are as defined in Eq.(11)

The coupled perturbed lateral equations of motion in the frequency-domain can be written as

$$A\tilde{x}=B \quad (18)$$

$$\tilde{z}=C\tilde{x} \quad (19)$$

where $\tilde{x}$ and $\tilde{z}$ are respectively the state and output vectors. A and B are the system matrices and C is the observation matrix.

$$\tilde{x}=[\tilde\beta/\tilde\delta_a,\ \tilde p/\tilde\delta_a,\ \tilde r/\tilde\delta_a,\ \tilde\phi/\tilde\delta_a]^T$$

$$\tilde{z}=[\tilde\beta/\tilde\delta_a,\ \tilde p/\tilde\delta_a,\ \tilde r/\tilde\delta_a,\ \tilde a_y/\tilde\delta_a]^T$$

The system matrices in Eq. 18—19 are formulated as

$$
A=\begin{bmatrix}
j\omega-k_1(Cy_{\beta})ss & -k_2(Cy_{p})ss & 1-k_2(Cy_{r})ss & -k_7 \\
-k_3(C_{l_{\beta}})ss & j\omega-k_4(C_{l_p})ss & -k_4(C_{l_r})ss & 0 \\
k_5(Cn_{\beta})ss & -k_6(Cn_{p})ss & j\omega-k_6(Cn_{r})ss & 0 \\
0 & -1 & 0 & j\omega
\end{bmatrix}
$$

$$
B=\begin{bmatrix}
k_1(Cy_{\delta_r})ss & k_1[(Cy_{\delta_a})ss-k_8P_1] \\
k_3(C_{l_{\delta_r}})ss & k_3[(C_{l_{\delta_a}})ss-k_{10}P_1-k_9P_2] \\
k_5(Cn_{\delta_r})ss & k_5[(Cn_{\delta_a})ss+k_{11}P_1] \\
0 & 0
\end{bmatrix}
$$

$$
C=\begin{bmatrix}
1 & 0 & 0 & 0 \\
0 & 1 & 0 & 0 \\
0 & 0 & 1 & 0 \\
0 & 0 & 0 & 1 \\
j\omega/k_7 & 0 & 1/k_7 & -1
\end{bmatrix}
$$

where

$$\widetilde{P}_1 = a_V \left(\frac{d\sigma}{d\delta_a}\right)_{ss} \left[1-\widetilde{D}_1(j\omega)\right]$$

$$\widetilde{P}_2 = a_t \left(\frac{d\epsilon}{d\alpha}\right)_{l,ss} \alpha_\delta \left[1-\widetilde{D}_2(j\omega)\right]$$

and constants k_1 to k_{11} are defined as

$k_1=\rho uS_W/2m$ $\quad k_2=\rho bS_W/4m$

$k_3=\rho bS_W u^2/2I_x$

$k_4=\rho uS_W b^2/4I_x$ $\quad k_5=\rho u^2S_W b/2I_z$

$k_6=\rho uS_W b^2/4I_z$

$k_7=g/u$ $\quad k_8=S_V/S_W$ $\quad k_9=2S_t\overline{y}/S_W b$

$k_{10}=S_V z_V/S_W b$ $\quad k_{11}=S_V l_V/S_W b$

Results and Discussion

An example airplane similar to the one used in ref. 5 was considered. The computer generated frequency response curves with unsteady aerodynamic modelling, obtained from Eq.(19) for a unit impulse aileron input, were used as measured responses. To asses the contribution of unsteady effects, these measured responses were compared with responses generated without inclusion of unsteady effects. Such a comparison for the yaw rate ($\widetilde{r}$) in Fig. 4 shows a significant contribution of unsteadiness. Similar observations were also made for other output variables like $\widetilde{\beta}$, $\widetilde{p}$ and $\widetilde{a}_y$. Next, responses were generated wherein the load build up part of the unsteady aerodynamic effects was omitted. As illustrated in Fig. 4 for yaw rate, the close matching of such a response with the one which includes complete unsteadiness suggests that the contribution due to the load build up effects is insignificant; this justified omitting of the load build up effects from the equations of motion.

The parameters were estimated from the simulated flight data (for $\Lambda=0°$) while retaining the unsteady aerodynamic modelling in the estimation algorithm. As expected for simulated case, the

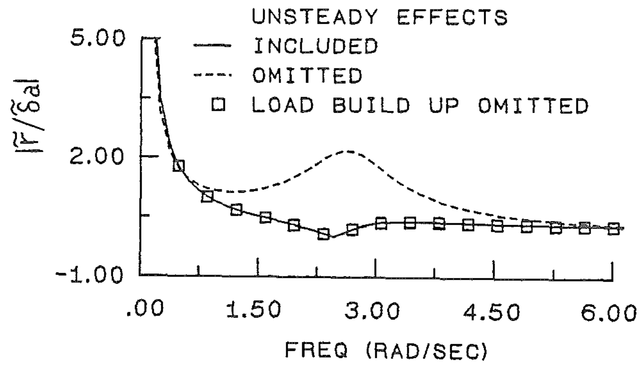

FIG.4 COMPARISON OF MEASURED RESPONSE WITH AND WITHOUT UNSTEADY EFFECTS

estimated parameters compared exactly with their true values (see column 3 of Table I). The measured and estimated responses also matched well for all the observation variables.

More interesting case was to omit the unsteady aerodynamic modelling from the estimation algorithm and thereby observe how the unsteady effects present in the flight data get absorbed in estimated equivalent parameters. Parameter extraction was performed in two different modes

Mode I where only time-lag effects were omitted from the estimation algorithm $(\widetilde{D}_1=\widetilde{D}_2=0)$

Mode II where unsteady aerodynamic modelling was altogether omitted from the estimation algorithm $(\widetilde{P}_1=\widetilde{P}_2=0)$

It may be noted that the simulated measured responses used for mode I and II always contained complete unsteady effects.

The estimated parameters for mode I (column 4) and mode II (column 5) are given in Table I. It may be seen that only the aileron control derivatives Cy_{δ_a}, $C_{l_{\delta_a}}$ and Cn_{δ_a} show significant difference between mode I and mode II ; specifically, Cy_{δ_a} even showing a change of sign. However, when a comparison was made of the estimated responses for mode I and mode II, the variations between the two were insignificant as may be seen in Fig. 5. This intriguing contradiction at first instance could be explained by defining the *equivalent estimated derivatives* as follows.

From Matrix B of Eq.(18), the frequency dependent control derivatives are given by

$$C'_{y_{\delta_a}} = (Cy_{\delta_a})ss - K_8\,P_2 \tag{20a}$$

$$C'_{l_{\delta_a}} = (C_{l_{\delta_a}})ss - K_{10}\,P_2 - K_9\,P_3 \tag{20b}$$

$$C'_{n_{\delta_a}} = (Cn_{\delta_a})ss + K_{11}\,P_2 \tag{20c}$$

The equivalent estimated derivatives for mode I are defined with $\widetilde{D}=0$ in Eq.(20), and are written as

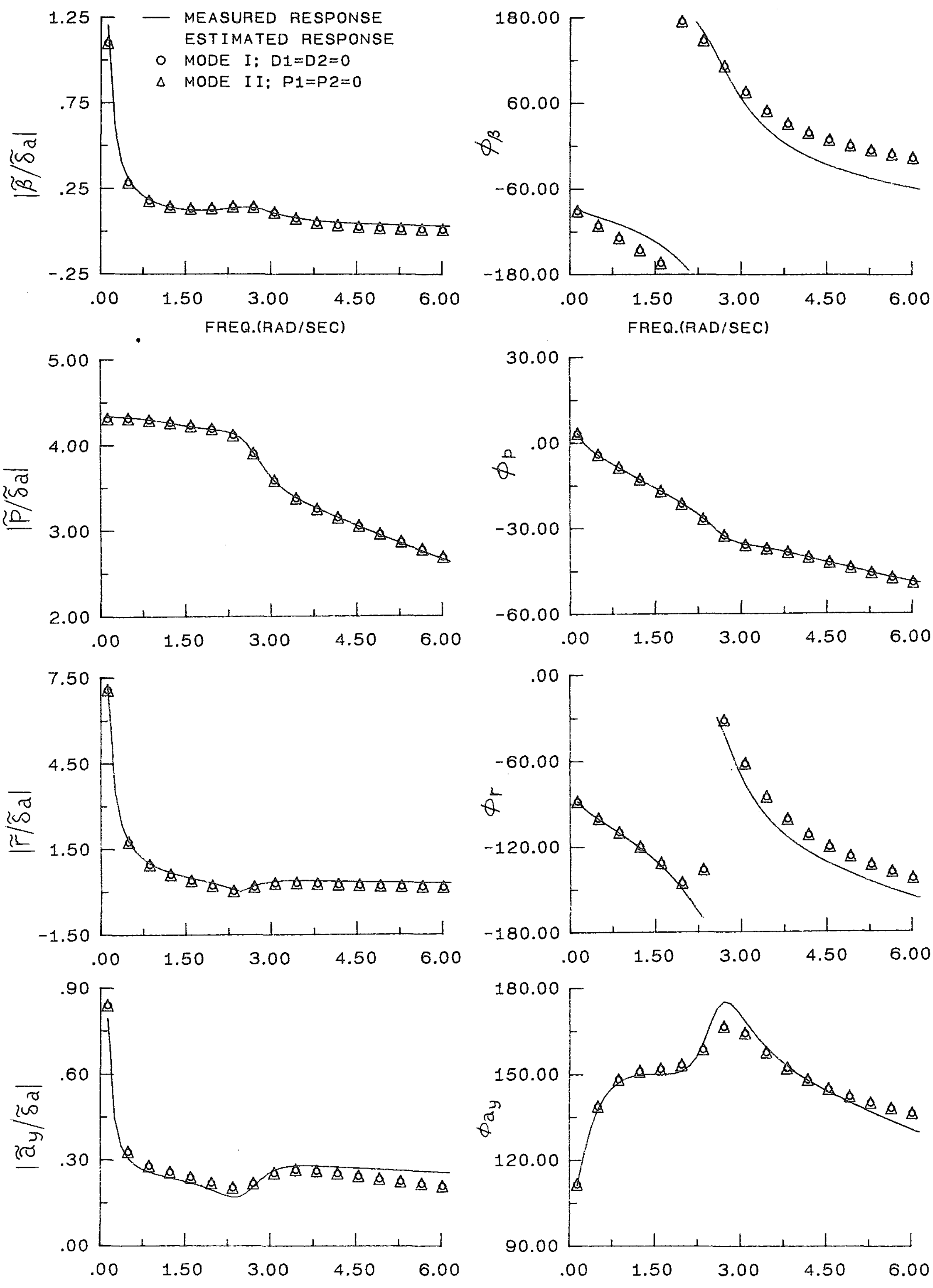

FIG. 5 COMPARISON OF ESTIMATED RESPONSE FOR MODE I AND MODE II WITH MEASURED RESPONSE

$$C''_{y_{\delta_a}} = (C_{y_{\delta_a}})_{ss} - K_8\, a_v \left(\frac{d\sigma}{d\delta_a}\right)_{ss} \tag{21 a}$$

$$C''_{l_{\delta_a}} = (C_{l_{\delta_a}})_{ss} - K_{10}\, a_v \left(\frac{d\sigma}{d\delta_a}\right)_{ss} - K_9\, a_t \left(\frac{d\epsilon}{d\alpha}\right)_{l,ss} \alpha_\delta \tag{21 b}$$

$$C''_{n_{\delta_a}} = (C_{n_{\delta_a}})_{ss} + K_{11}\, a_v \left(\frac{d\sigma}{d\delta_a}\right)_{ss} \tag{21 c}$$

Similarly, the equivalent estimated derivatives for mode II are defined with $\widetilde{P}=0$ in Eq.(20), and these are the same as the steady state derivatives appearing as the first term on right hand side of Eq.(20).

The equivalent estimated control derivatives for mode I are shown in column 6 of Table I while the equivalent derivatives for mode II are the same as listed in column 5 of Table I. A comparison of these equivalent derivatives shows that not only the sign discrepancy of $C_{y_{\delta_a}}$ has disappeared but also the numerical values are close to each other. This explains the apparent anamoly observed between the estimated values and corresponding responses for mode I and mode II.

As seen from Table I, for the aileron control derivatives, a comparison of the true values (column 2) and equivalent estimated values (columns 5 and 6) shows that the change in $C_{l_{\delta_a}}$ values is quite insignificant as compared to changes in $C_{y_{\delta_a}}$ and $C_{n_{\delta_a}}$ values. To explain this, a comparison of unsteady contributions due to downwash at horizontal tail and sidewash at vertical tail was carried out. Figure 6 illustrates the relative contributions to roll rate. As seen from Fig. 6, the response with downwash effects only is close to the true response, and thereby suggests that contributions to $C_{l_{\delta_a}}$ due to downwash effects are small for the airplane considered. A large horizontal tail may, however, lead to downwash effects being comparable to unsteady effects in sidewash and thus also affect the $C_{l_{\delta_a}}$ values significantly.

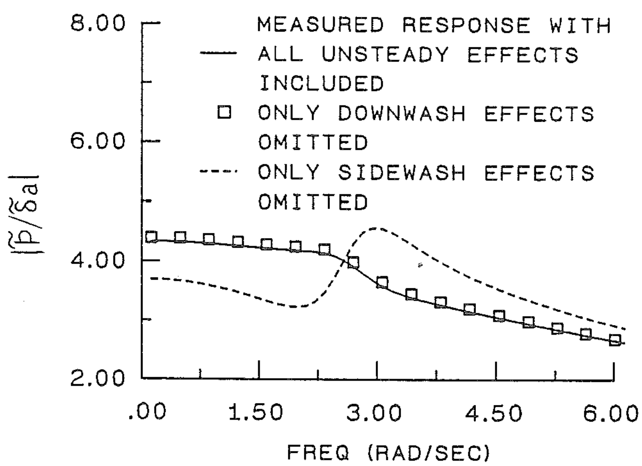

FIG.6 COMPARISON OF MEASURED RESPONSES WITH UNSTEADY EFFECTS IN DOWNWASH AND/OR SIDEWASH

Conclusions

A simplified vortex model has been developed to account for unsteady aerodynamic effects due to aileron deflections. Parameters have been extracted in two different modes, omitting, respectively, the time

Parameters	True Value	Estimated Parameters						Equivalent estimated Derivatives ; Eq.(21)
		Unsteady Effects Included		Mode I $\widetilde{D}_1=\widetilde{D}_2=0$		Mode II $\widetilde{P}_1=\widetilde{P}_2=0$		
$-C_{y_\beta}$	0.3671	0.3671	(0)[a]	0.4337	(.0166)[a]	0.4346	(.0165)[a]	
$-C_{y_p}$	0.0400	0.0400	(0)	0.3973	(.0142)	0.3980	(.0141)	
$C_{y_{\delta_a}}$	0.0000	0.0000	(0)	0.1223	(.0177)	−0.0134	(.0051)	$C''_{y_{\delta_a}} = -0.0135$
$-C_{l_\beta}$	0.1231	0.1231	(0)	0.1790	(.0078)	0.1782	(.0078)	
$-C_{l_p}$	0.5320	0.5320	(0)	0.5949	(.0017)	0.5950	(.0017)	
C_{l_r}	0.1706	0.1706	(0)	0.2357	(.0133)	0.2341	(.0134)	
$C_{l_{\delta_a}}$	0.2590	0.2590	(0)	0.2761	(.0005)	0.2597	(.0005)	$C''_{l_{\delta_a}} = 0.2598$
C_{n_β}	0.1474	0.1474	(0)	0.1909	(.0025)	0.1908	(.0025)	
$-C_{n_p}$	0.0420	0.0420	(0)	−0.0852	(.0015)	−0.0852	(.0015)	
$-C_{n_r}$	0.2404	0.2404	(0)	0.2803	(.0075)	0.2798	(.0075)	
$-C_{n_{\delta_a}}$	0.0250	0.0250	(0)	0.0715	(.0007)	0.0088	(.0007)	$-C''_{n_{\delta_a}} = 0.00886$

[a]Cramer–Rao bounds

TABLE 1 COMPARISON OF PARAMETER ESTIMATES FOR DIFFERENT ESTIMATION MODELS lag effects and the steady state vortex system in estimation model for mode I and mode II. For the airplane considered, the estimated derivatives show a marked variation from their true values. Significant difference between the values of the aileron control derivatives extracted in mode I and mode II was also observed and an explanation is offered by invoking the concept of equivalent derivatives. A brief study suggests that the induced sidewash effects are more pronounced than the downwash effects.

References

[1] Wells, W.R. and Queijo, M.J., "Simplified Unsteady Aerodynamic Concepts with Application to Parameter Estimation," *J. of Aircraft*, Vol. 16, No. 2, Feb. 1979, pp. 90–94 .

[2] Queijo, M.J., Wells, W.R. and Keskar, D.A. , "Approximate Indicial Lift Function for Tapered Swept Wings in Incompressible Flow," *NASA TP*–1241, 1978 .

[3] Queijo, M.J., Wells, W.R. and Keskar, D.A. , "Inclusion of Unsteady Aerodynamics in Longitudinal Parameter Estimation from Flight Data," *NASA Tech. Paper* 1536 , 1979 .

[4] Raisinghani, S.C. and Ghosh, A.K. , "Parameter Estimation of an Augmented Airplane with Unsteady Aerodynamic Modelling," *Proceedings of the 17th Int. Symp. on Space Tech. and Science*, Tokyo, Japan , 20–25 May, 1990, pp. 699–706.

[5] Singh, J. and Raisinghani, S.C. , "Unsteady Aerodynamic Modelling for Aircraft Lateral Parameter Estimation," *The Aeronautical Journal*, Vol. 95, March 1991, pp. 88–94 .

[6] Wells, W.R., Banda, S. and Quam, D.L. , "Aircraft Lateral Parameter Estimation from Flight Data with Unsteady Aerodynamic Modelling," *Proceedings of the 19th AIAA Aerospace Sciences Meeting*, St. Louis , Mo. , Jan. 12–15 , 1981 .

[7] Roskam, J. , *Methods for Estimating Stability and Control Derivatives for Conventional Subsonic Airplanes*, Roskam Aviation and Engineering Corporation, 1973.

[8] Hoak, D.E., Ellison, D.E. et al. , *USAF Stability and Control DATCOM*, Flight Control Division ; Airforce Flight Dynamics Laboratory, Wright Patterson Air Force Base, Ohio, 1960, revised 1975.

[9] Abromowitz, M. and Stegun, I.A. , *Handbook of Mathematical Functions with Formulas, Graphs and Mathematical Tables*, Dover Publications, New York, 1965, pp. 228–237.

APPENDIX A

The function $f_1,\ldots,f_4$ represent the contribution of bound, shed and trailing vortices of the left panel of the wing to the sidewash at the a.c. of the vertical tail.

$$f_1(t) = \left[\{m_1+(m_3/m_4)\sin\Lambda\} + \frac{b}{2m_4}\cos\Lambda\right]\sin\Lambda / h_1^2$$

$$f_2(t) = -\left[\frac{(l_v-m_2)\sin\Lambda}{m_5} + \frac{m_1+m_2}{m_6}\sin\Lambda + \left(\frac{b}{2m_6}\cos\Lambda\right)\right] / h_2^2$$

$$f_3(t) = \left[\frac{(m_1+m_2)}{m_6} - \frac{m_1}{m_4}\right] / h_3^2$$

$$f_4(t) = -\left[m_3+(m_2-l_v)/m_5\right] / z_v^2$$

where

$$m_1 = \frac{b}{2}\tan\Lambda - l_v \qquad m_2 = c_r + \frac{ut}{2}$$

$$m_3 = \frac{l_v}{\sqrt{l_v^2+z_v^2}} \qquad m_4 = \sqrt{m_1^2+(b/2)^2+z_v^2}$$

$$m_5 = \sqrt{(l_v-m_2)^2+z_v^2} \qquad m_6 = \sqrt{(m_1+m_2)^2+(b/2)^2+z_v^2}$$

$$h_1 = \sqrt{(l_v\cos\Lambda)^2+z_v^2} \qquad h_2 = \sqrt{[(l_v-m_2)\cos\Lambda]^2+z_v^2}$$

$$h_3 = \sqrt{(b/2)^2+z_v^2}$$

For the vortex pattern in Fig. 1, the upwash at the a.c. of the right panel of the horizontal tail will be equal to the downwash on the left panel of the horizontal tail.

APPENDIX B

In the expressions that follow, the contribution to downwash at the a.c. of the left horizontal tail by the bound, shed and trailing vortices is given by g_i for the vortex pattern of the left panel of the wing and g_{i+4} for that of the right panel (i=1,2,3) . Function g_4 represents the contribution of the center trailing vortex to the downwash.

$$g_i(\bar{y},t) = (-1)^{i+1}\left[\cos A_i + \cos B_i\right] / h_i \quad i=1,2,3$$

$$g_{i+4}(\bar{y},t) = -g_i(-\bar{y},t) \qquad i=1,2,3$$

where

$$\cos A_1 = (m_1\sin\Lambda + m_3\cos\Lambda)/m_4$$

$$\cos B_1 = (l\sin\Lambda + \bar{y}\cos\Lambda)/m_6$$

$$\cos A_2 = \left[(m_1+m_2)\sin\Lambda + m_3\cos\Lambda\right]/m_5$$

$$\cos B_2 = \left[(l-m_2)\sin\Lambda + \bar{y}\cos\Lambda)\right]/m_7$$

$$\cos A_3 = -m_1/m_4 \qquad \cos B_3 = (m_1+m_2)/m_5$$

and

$$h_1 = |l\cos\Lambda - \bar{y}\sin\Lambda| \qquad h_2 = |(l-m_2)\cos\Lambda - \bar{y}\sin\Lambda|$$

$$h_3 = |m_3|$$

The function $g_4(\bar{y},t)$ is given by

$$g_4(\bar{y},t) = \frac{1}{\bar{y}}\left[\frac{l}{m_6} - \frac{l-m_2}{m_7}\right]$$

For convinience, constants m_1 to m_3 are defined as

$$m_1 = \frac{b}{2}\tan\Lambda - l \qquad m_2 = c_r + \frac{ut}{2}$$

$$m_3 = \frac{b}{2} - \bar{y} \qquad m_4 = \sqrt{m_1^2+m_3^2}$$

$$m_5 = \sqrt{(m_1^2+m_2^2)+m_3^2} \qquad m_6 = \sqrt{l^2+\bar{y}^2}$$

$$m_7 = \sqrt{(l-m_2)^2+\bar{y}^2}$$

For the vortex pattern in Fig. 1, the induced upwash at the a.c. of the right panel is equal to the downwash on the left panel of the horizontal tail.